The influence of a second-order phase transition on impurity luminescence: A study of $RbCdF_3:Mn^{2+}$

1994 J. Phys.: Condens. Matter 6 6353

(http://iopscience.iop.org/0953-8984/6/31/034)

J. Phys.: Condens. Matter 6 (1994) 6353–6366. Printed in the UK

The influence of a second-order phase transition on impurity luminescence: a study of $RbCdF_3:Mn^{2+}$

M C Marco de Lucas†, F Rodríguez†, M Moreno† and A Tressaud‡

† DCITTYM (Sección Ciencia de Materiales), Facultad de Ciencias, Universidad de Cantabria, 39005 Santander, Spain

‡ Laboratoire de Chimie du Solide du CNRS, Université de Bordeaux I, 33405 Talance, France

Received 9 February 1994

Abstract. Precise photoluminescence measurements have been carried out on $RbCdF_3:Mn^{2+}$ in the 9–300 K range to explore the structural phase transition of the host lattice at $T_c = 124$ K using the first (M_1) and second (M_2) moments of the emission band together with the lifetime τ as probes. Aside from showing a sensitivity of $M_2(T)$ and $\tau(T)$ to the phase transition, the present data reveal that the curve $M_1(T)$ experiences a small but observable change of slope in the vicinity of T_c. It is demonstrated that this jump, $\Delta_t(\partial M_1/\partial T)_P = 0.22\ cm^{-1}\ K^{-1}$, is mainly associated with the increase experienced by the local thermal expansion coefficient below T_c. The importance of both the implicit and explicit contributions to $M_1(T)$ is analysed throughout this work.

Neither the luminescence nor the excitation spectrum shows any evidence of tetragonal distortion in the MnF_6^{4-} complex. This fact is explained through the $R_{ax} - R_{eq} = 0.2$ pm value (where R_{ax} and R_{eq} are the axial and equatorial Mn^{2+}–F^- distances) at 30 K, and the coupling coefficient $V_E = 66\ cm^{-1}\ pm^{-1}$ with the E_g Jahn–Teller mode of MnF_6^{4-}. Finally, we have found that this crystal exhibits photochemical reactions under UV light irradiation, leading to the formation of centres that transfer easily to Mn^{2+} ions. These centres give rise to an intense absorption band at 310 nm, analogously to those previously formed under x-irradiation.

1. Introduction

Because of their high symmetry, cubic fluoroperovskites have been employed as host lattices of divalent transition-metal impurities [1–7] in order to achieve a detailed correlation among their optical and EPR spectra and the local structure displayed around the impurity.

In the case of Mn^{2+}-doped fluoroperovskites, for instance, the actual Mn^{2+}–F^- distance, R, at room temperature has been determined from the analysis of the experimental isotropic superhyperfine constant, A_s [8], and optical excitation spectra [6, 7].

With the exception of $KMgF_3$, $KZnF_3$, $CsCdF_3$ and $CsCaF_3$, the remaining fluoroperovskites undergo one or more structural phase transitions (PTs) below room temperature. These phase transitions mainly involve rotations of the MF_6^{4-} (M =divalent cation) octahedra leading to a local tetragonal distortion of the F octahedra [9–13]. In fact, such transitions are associated with the condensation of the acoustical R_{25} or M_3 phonons, whose frequency becomes zero at the transition temperature. An $O_h^1 \rightarrow D_{4h}^{18}(RbCdF_3)$ or an $O_h^1 \rightarrow D_{4h}^5(KMnF_3)$ structural phase transition takes place depending on which mode, R_{25} or M_3, is involved. A conspicuous example of this behaviour is $RbCdF_3$, which experiences an $O_h^1 \rightarrow D_{4h}^{18}$ structural phase transition of second-order character at 124 K [12], giving rise to two different distances, called R_{eq}^0 and R_{ax}^0, between a Cd^{2+} ion and the nearest F^-

0953-8984/94/316353+14$19.50

ions. At 30 K it can be inferred that $R^0_{ax} = 220.4$ pm and $R^0_{eq} = 219.3$ pm through the experimental lattice parameters, $c = 440.9$ pm and $a = 437.5$ pm, using Allelfed's model [14].

As regards an Mn^{2+} impurity in the tetragonal phase of $RbCdF_3$, precise information on its local geometry can be reached by analysing the good ENDOR data obtained at $T = 30$ K by Studzinski and Spaeth [4]. These authors report $A_s(ax) = 15.80(3) \times 10^{-4}$ cm^{-1} and $A_s(eq) = 15.93(3) \times 10^{-4}$ cm^{-1} for axial and equatorial ligands, respectively. Using the procedure explained in [8] a value $R_{ax} - R_{eq} = 0.2$ pm is found from the experimental superhyperfine constants. This latter value, which is certainly much smaller than $R^0_{ax} - R^0_{eq} = 1.1$ pm, stresses that local changes around an impurity can be different from those for the perfect lattice. Having in mind this previous characterization of $RbCdF_3$:Mn^{2+} in the tetragonal phase, the detection of the $O^1_h \rightarrow D^{18}_{4h}$ PT in $RbCdF_3$:Mn^{2+} using the optical properties of the Mn^{2+} impurity as a probe does not seem to be a simple task. This difficulty is underlined by recent results on $RbCdF_3$:Cr^{3+} where no evidence of the PT was found from the optical spectra of Cr^{3+} [5].

The main goal of this work is to investigate the optical excitation and luminescence spectra of $RbCdF_3$:Mn^{2+} single crystals, and their temperature dependence in the 9–300 K range. Special emphasis is paid on the sensitivity or lack of sensitivity of Mn^{2+} spectra to detect the PT undergone by the $RbCdF_3$ crystal. Therefore the present work can be considered as an exploration on the *limits of optical probes* for detecting PTs in insulators. It is worth noting that these optical probes are known to be very sensitive for detecting PTs with a strong first-order character where jumps of distances between closest ions of the order of 1 pm are involved [7, 15, 16].

Another drawback for carrying out the present task comes from the formation of some *centres* that strongly absorb around 310 nm. The nature of such centres, first discovered by irradiating with x-rays $RbCdF_3$ samples either nominally pure or doped with divalent TM impurities, remains unknown [17]. We have found that these centres are also formed under irradiation with UV light as explained in subsection 3.1. Their presence in the $RbCdF_3$:Mn^{2+} crystal makes it difficult to detect the excitation spectrum of isolated Mn^{2+} ions given that a strong Mn^{2+} emission is induced upon excitation of the UV band of these centres. This difficulty has been overcome using crystals *free* from centres and avoiding excitation in the UV region. Therefore, the study of the optical properties of the isolated Mn^{2+} has been followed mainly by the changes experienced by the emission band and the associated lifetime, τ, employing the 514.5 nm line of an Ar laser. This radiation completely avoids the formation of centres and allows us to populate the first $^4T_{1g}(G)$ excited state of Mn^{2+} in $RbCdF_3$, which is located at 512 nm at room temperature.

2. Experimental details

Single crystals of $RbCdF_3$:Mn^{2+} were grown by the Bridgman method from RbF and CdF_2 commercial products with 99.99% purity and a mixture of 1% MnF_2 + RbF in the powdered sample. The melting temperature was determined by DTA ($T_F = 1290$ K). The crystal growth equipment was composed of two independent furnaces, which were isolated by an insulating zone. The temperature could be therefore separately programmed in each part. About 30 g of material were introduced under Ar gas into a Pt crucible. The material was heated up to 50 K above the melting point and then allowed to cool down to room temperature at a rate of 5 K h^{-1}.

The real Mn^{2+} concentration in the samples employed in the present work, 2500 ± 500 ppm, was determined by comparing the EPR integrated intensity at room temperature of our $RbCdF_3:Mn^{2+}$ powdered samples with a $KZnF_3:Mn^{2+}$ (2%) pattern.

To obtain the excitation and emission spectra of $RbCdF_3:Mn^{2+}$ as well as to carry out lifetime measurements it was compulsory to improve the sensitivity of the detection because of the low value of the Mn^{2+} concentration.

Excitation spectra were obtained with an implemented Jobin Yvon JY-3D fluorimeter [18] equipped with a photon counting technique. The excitation beam from an Xe lamp (150 W) was chopped and focused on the sample. The luminescence signal was detected with a Hamamatsu R928 photomultiplier and measured during the non-excitation periods with a Stanford System SR440 preamp and SR 400 photon counter.

Luminescence spectra were obtained by means of a Jobin Yvon HR-320 monochromator employing the chopped light of a Spectra Physics model 2020-03 Ar laser ($\lambda = 514.5$ nm) as excitation source. For lifetime measurements, the luminescence signal was digitized by means of a Tektronix 2430A scope.

Temperature variations were achieved by a Scientific Instruments DE-202 closed-circuit cryostat allowing temperature stabilities within 0.1 K and an accuracy of 0.5 K, with an APD-K temperature controller.

3. Results and discussion

3.1. UV-induced radiation damage

Mn^{2+}-doped fluoroperovskites exhibit a weak luminescence from the first $^4T_{1g}(G)$ excited state of the Mn^{2+} in the 500–600 nm range at room temperature. For $RbCdF_3:Mn^{2+}$, the intensity of this luminescence, peaking at 560 nm can be increased by several orders of magnitude by irradiating with x-rays or, as we have found, with UV light. Enhancements of the luminescence in doped fluoroperovskites were also observed in $KMgF_3$ doped with Mn^{2+} and Co^{2+} by electron irradiation, though profound changes in both the emission and the excitation spectra of Mn^{2+} were detected in these systems [19].

These photochemical effects in $RbCdF_3:Mn^{2+}$ make difficult to obtain the excitation spectra of isolated Mn^{2+} due to the radiation-induced damage when exciting with UV light. This phenomenon is clearly illustrated by the excitation spectra of figure 1. Spectrum (a) corresponds to an $RbCdF_3:Mn^{2+}$ sample after being irradiated with 230 nm light for 30 min. It can be seen that the excitation spectrum corresponding to isolated Mn^{2+} ions is practically invisible, being essentially masked by a broad band centred at 310 nm with a bandwidth at half maximum of 7000 cm^{-1}. At variance with the Mn^{2+} crystal-field peaks, this excitation band is also observed in the optical absorption spectrum of $RbCdF_3:Mn^{2+}$ (figure 2). Its intensity increases with the UV dose and is very similar to that previously found in $RbCdF_3$ samples (either nominally pure or doped with Ni^{2+}, Co^{2+} or Mn^{2+}) by Losada *et al* [17], after x-ray irradiation. Thus the present results indicate that the same centre (whose structure is currently unknown) is also formed by irradiation with UV light.

Excitation into the 310 nm band induces a strong Mn^{2+} luminescence as well as a progressive diminution of this absorption band, which is related to the destruction of the centres discussed. Moreover, the presence of these centres is associated with the persistent Mn^{2+} luminescence (phosphorescence) exhibited by these crystals. The corresponding lifetime is about 15 min at room temperature. This phosphorescence, due to a centre$\rightarrow Mn^{2+}$ energy transfer process, is thermally activated, as is evidenced in the thermoluminescence curve of figure 3. We have verified that the spectrum of the emitted light in this process

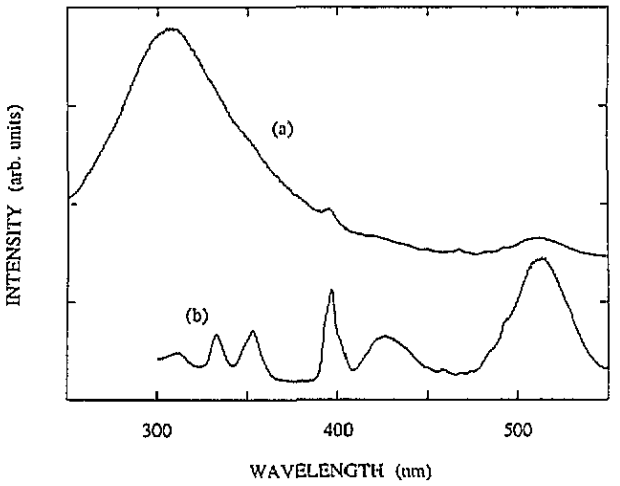

Figure 1. The room-temperature excitation spectra of $RbCdF_3:Mn^{2+}$ (λ_{em} = 580 nm). Spectrum (a) was obtained after sample irradiation with 230 nm light for 30 min. Spectrum (b) corresponds to the annealed sample.

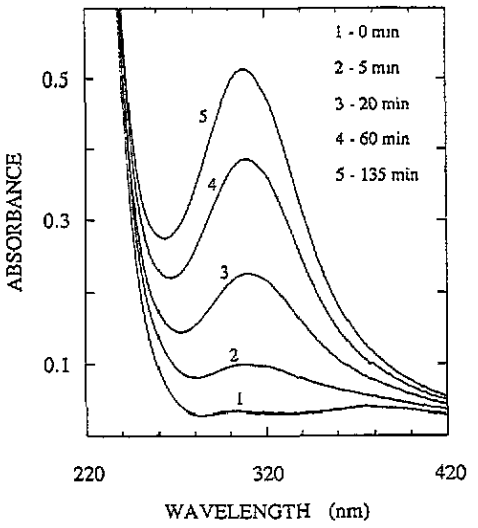

Figure 2. The variation of the optical absorption spectra in the UV range of an annealed $RbCdF_3:Mn^{2+}$ sample with irradiation time.

corresponds only to the Mn^{2+} emission as the emission spectrum at room temperature due to the thermoluminescence process gives rise to the same band, associated with isolated Mn^{2+} ions in $RbCdF_3$ (peaked at 560 nm), and discussed in the next section. Also we have verified that upon heating at about 400 °C, the emission associated with the thermoluminescence peaks at 560 nm. Four peaks are observed at 250, 290, 340 and 370 °C. Heating of the crystals above these temperatures causes a drastic reduction of the UV-induced centres. In fact, the excitation and the corresponding 310 nm absorption band disappear completely

after annealing the UV-irradiated $RbCdF_3:Mn^{2+}$ crystals at 400 °C. The remaining excitation spectrum shown in figure 1(*b*) fully corresponds to the isolated Mn^{2+} ions. We have not further investigated the nature of traps giving rise to the thermoluminescence spectrum of figure 1 as it lies beyond the central purpose of this research.

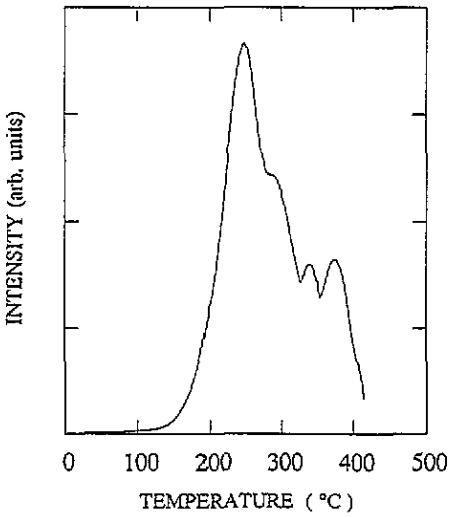

Figure 3. The thermoluminescence curve of an irradiated $RbCdF_3:Mn^{2+}$ sample. The luminescence intensity corresponds to Mn^{2+} ($\lambda_{em} = 560$ nm). Heating rate, 3 K min^{-1}.

3.2. Temperature dependence of the optical spectra

Figure 4 shows the excitation and luminescence spectra of an annealed $RbCdF_3:Mn^{2+}$ crystal at 300 and 9 K. The transition energies and the crystal-field peak assignment within an O_h scheme are given in table 1. It is worth noting that the emission peak experiences a larger shift than the $^6A_{1g}(S) \rightarrow {}^4T_{1g}(G)$ excitation peak, which is usually the most sensitive to changes of Mn^{2+}–F^- distances and temperature among the observed crystal-field transitions of MnF_6^{4-} [7]. A similar situation has recently been encountered in the photoluminescence study of Na_6MnX_8 (X = Cl, Br) compounds, where the origin of the different shifts undergone by the emission and the corresponding excitation peak has been analysed [20].

The study of the temperature dependence of the optical spectra of isolated Mn^{2+} has been focused mainly on the luminescence band induced by exciting with light of 514.5 nm. This is due to the larger shift experienced by luminescence band from 300 to 9 K and also to the fact the 514.5 nm excitation light avoids completely the formation of unwanted centres.

Figure 5 depicts the luminescence spectra of $RbCdF_3:Mn^{2+}$ recorded at different temperatures. It can be seen that the spectra recorded just above and below the PT temperature, $T_c = 124$ K, are very similar. No splitting associated with the tetragonal distortion has been detected either in the luminescence or in the excitation spectra.

A vibronic structure similar to that found for Mn^{2+}-doped $KMgF_3$ and $KZnF_3$ [21] is resolved around the origin of the emission spectrum of $RbCdF_3:Mn^{2+}$ at 9 K (inset of figure 5). The presence of a zero-phonon line at 18 360 cm^{-1} and a false origin at 265 cm^{-1}

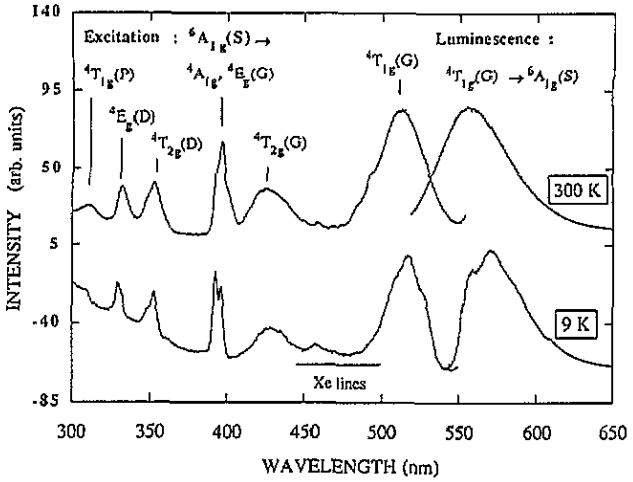

Figure 4. The excitation and luminescence spectra of $RbCdF_3:Mn^{2+}$ at 300 and 9 K. The peaks were labelled according to the O_h symmetry of the MnF_6^{4-}.

Table 1. The transition energies and crystal-field band assignment of the $RbCdF_3:Mn^{2+}$ excitation and emission spectra at 300 and 9 K. The B and C Racah parameters and 10Dq were obtained by the standard procedure including Trees and seniority corrections: $\alpha = 65\ cm^{-1}$ and $Q = -131\ cm^{-1}$. Energies are in cm^{-1}.

	Transition energy	
Assignment	300 K	9 K
Excitation		
$^4T_{1g}(G) \leftarrow {}^6A_{1g}(S)$	19510	19275
$^4T_{2g}(G)$	23470	23190
$^4A_{1g}, ^4E_g(G)$	25215	25355
$^4T_{2g}(D)$	28335	28385
$^4E_g(D)$	30045	30330
$^4T_{1g}(P)$	32530	—
Emission		
$^4T_{1g}(G) \rightarrow {}^6A_{1g}(S)$	17950	17550
B	813	815
C	3157	3181
10Dq	7264	7748

is noteworthy. Vibrational peaks are found at energies from the zero-phonon line similar to the phonon energies at the Brillouin zone edge and Γ, measured for $CsCaF_3$ and $RbCaF_3$ [22–24]. A full account of the behaviour of zero-phonon lines, vibronic structure and Stokes shifts along the Mn^{2+}-doped fluoroperovskite series will be reported in the near future.

3.3. Variations undergone by the transition energy, bandwidth and lifetime of the luminescence band

In order to analyse the sensitivity of the optical properties for detecting the structural phase transition in $RbCdF_3:Mn^{2+}$, we have performed precise measurements of the emission

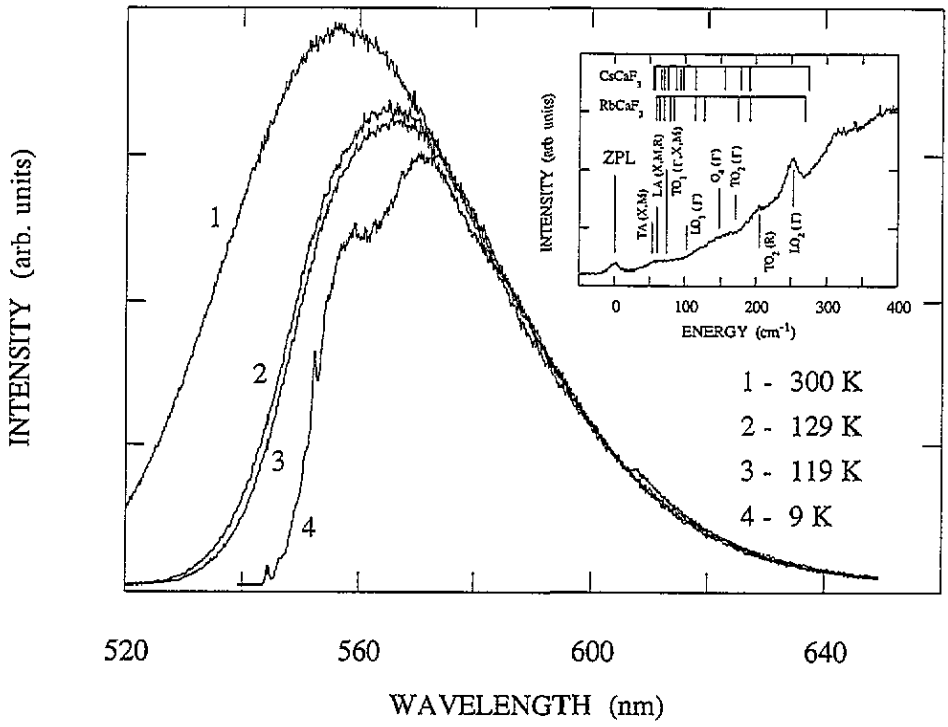

Figure 5. The luminescence spectra of $RbCdF_3:Mn^{2+}$ at different temperatures. The inset shows the vibronic spectra at $T = 9$ K. The peak labelling corresponds to phonons at the Brillouin zone edge and at Γ. Phonon energies from the zero-phonon line (ZPL) of $CsCaF_3$ and $RbCaF_3$ are included for comparison.

spectra and the corresponding lifetime in the 9–300 K range. The results are compared with those for $CsCaF_3:Mn^{2+}$, where the host lattice experiences no phase transition below 300 K (figures 6–8).

Figure 6 shows the variation of the first moment, M_1, of the emission band. The most salient feature is the small but detectable *jump of slope* experienced by M_1 in the vicinity of $T_c = 124$ K, at a pressure $P_0 = 0$ atm. In fact, from the data reported in figure 6, a value of $(\partial M_1/\partial T)_{P_0} = 1.88(5)$ cm^{-1} K^{-1} at $T = 145$ K in the cubic phase of $RbCdF_3$ can be obtained while a value of $(\partial M_1/\partial T)_{P_0} = 2.11(5)$ cm^{-1} K^{-1} is measured at $T = 100$ K in the tetragonal phase. Therefore, the jump of slope, $\Delta_t(M_1')$, that is actually measured in the present experiments, corresponds to

$$\Delta_t(M_1') = (\partial M_1/\partial T)_{P_0,T_c-t} - (\partial M_1/\partial T)_{P_0,T_c+t} \tag{1}$$

where $t \sim 20$ K. The value of $\Delta_t(M_1')$ is thus equal only to 0.23 cm^{-1} K^{-1} in the present case. Because of the small changes undergone by the slope it has not been possible to perform a proper measurement of the jump exactly at T_c (denoted as Δ_0). A microscopic analysis of $\Delta_t(M_1')$, similar to that observed for $RbCaF_3:Mn^{2+}$ at $T_c = 193$ K, is given in subsection 3.6.

Figures 7 and 8 display the temperature dependence of the emission bandwidth, H, derived from the second moment M_2 through $H = 2.36\sqrt{M_2}$, and the lifetime, τ,

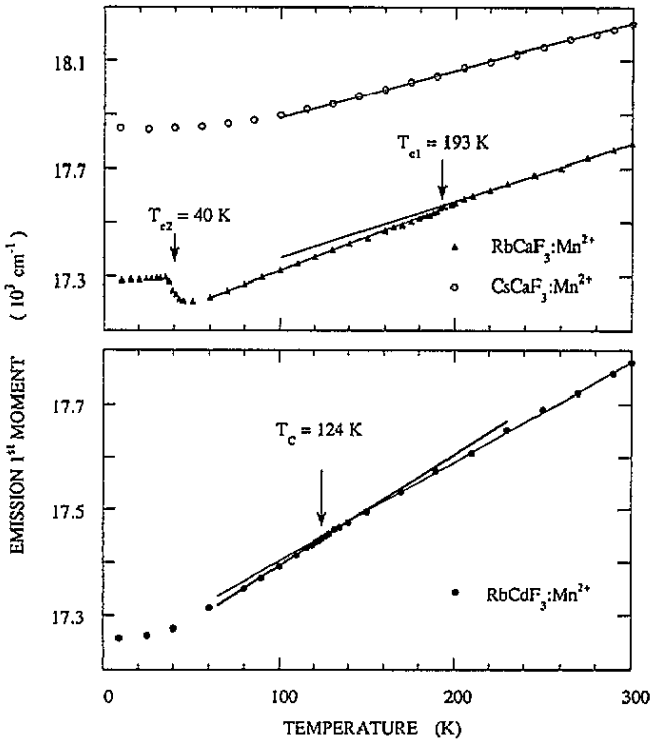

Figure 6. The temperature dependence of the emission first moment of $RbCdF_3:Mn^{2+}$ in the 9–300 K temperature range. The results are compared with those for $CsCaF_3:Mn^{2+}$ and $RbCaF_3:Mn^{2+}$. The arrows indicate the PT temperatures of these crystals. The straight lines are least-squares linear fits of $M_1(T)$ above and below T_c.

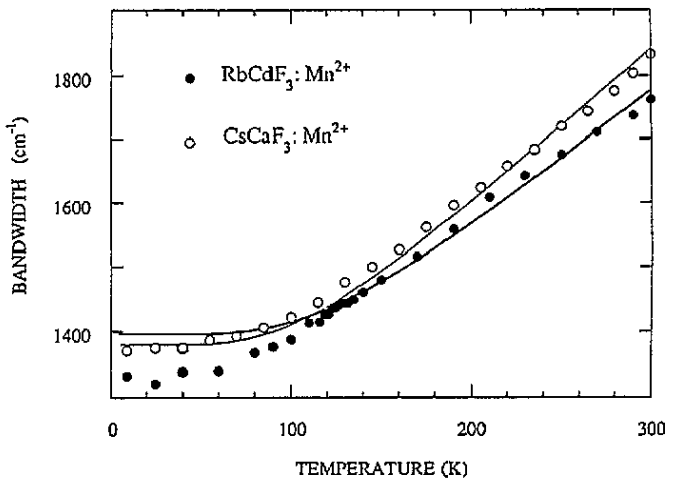

Figure 7. The variation of the emission bandwidth for $CsCaF_3:Mn^{2+}$ and $RbCdF_3:Mn^{2+}$ in the 9–300 K temperature range. The solid lines correspond to fits to (2).

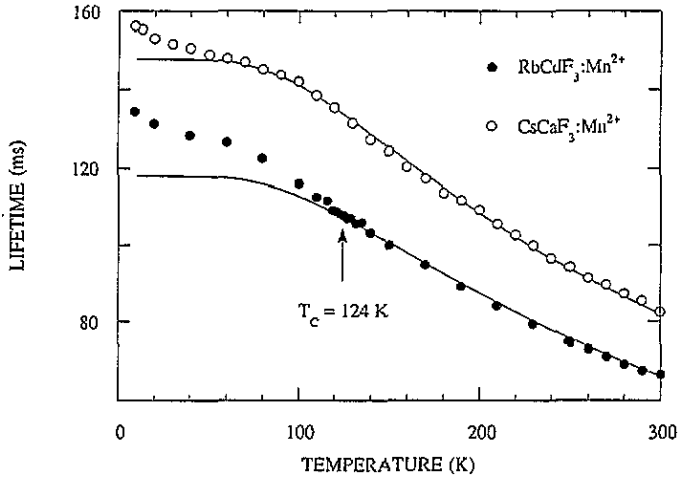

Figure 8. The variation of the lifetime for $CsCaF_3:Mn^{2+}$ and $RbCdF_3:Mn^{2+}$ in the 9–300 K temperature range. The solid lines correspond to fits to (3).

respectively. As regards the bandwidth, the experimental results for $CsCaF_3:Mn^{2+}$ can reasonably well fitted to a law

$$H(T) = H_0[\coth(\hbar\omega/2k_BT)]^{1/2} \tag{2}$$

in the *whole* temperature range with $H_0 = 1380\ cm^{-1}$ and $\hbar\omega = 267\ cm^{-1}$.

In the case of $RbCdF_3:Mn^{2+}$, the experimental H values for $T > 124$ K can be fitted to (2) with $H_0 = 1396\ cm^{-1}$ and $\hbar\omega = 302\ cm^{-1}$. The smaller Mn^{2+}–F^- distance, $R = 213$ pm, for $RbCdF_3:Mn^{2+}$ compared to $R = 215$ pm for $CsCaF_3:Mn^{2+}$ is quite consistent with the higher effective phonon frequency obtained for $RbCdF_3:Mn^{2+}$. Nevertheless, at variance with what is found for $CsCaF_3:Mn^{2+}$, the fitting given by (2) is *unable* to reproduce the experimental values found below the PT temperature. As the departure from the predictions given by (2) appears just below T_c, this fact can reasonably be related to the structural PT undergone by the host lattice.

As regards the temperature dependence of the experimental lifetime, it has been fitted to a law

$$\tau(T) = \tau_0 \tanh(\hbar\omega_u/2k_BT) \tag{3}$$

characteristic of electric dipole processes assisted by an odd phonon of frequency $\omega_u/2\pi$. For $CsCaF_3:Mn^{2+}$, the fitting parameters are $\tau_0 = 148$ ms and $\hbar\omega_u = 260\ cm^{-1}$. However, this fitting does not account for the slight lifetime increase observed below 50 K. The reason for this behaviour, also observed for Mn^{2+}-doped $KMgF_3$, $KZnF_3$ [21] and $RbCaF_3$ [7], is still unknown.

The lifetime values for $RbCdF_3:Mn^{2+}$ can also be well fitted to (3) with $\tau_0 = 118$ ms and $\hbar\omega_u = 265\ cm^{-1}$, but only above 124 K. Below this temperature τ clearly deviates from the predictions of (3), similarly to what was observed for the bandwidth.

3.4. Tetragonal splitting below T_c: relation with the Jahn–Teller constant V_E

Because of the tetragonal symmetry of $RbCdF_3$ below T_c, the first $^4T_{1g}(G)$ electronic state of MnF_6^{4-} should split into two states, $^4A_{1g}$ and ^4E_g, in a local D_{4h} symmetry. This splitting can

be estimated through the Jahn–Teller constant, V_E, which has been measured experimentally for the $^4T_1(G)$ state of $RbMnF_3$ [25], and also derived from the reduction of the spin–orbit splitting of the $^4T_{1g}(G)$ state in $KMgF_3:Mn^{2+}$ and $KZnF_3:Mn^{2+}$ [21].

The linear electron–phonon coupling term, H_{el-ph}, corresponding to a triplet state of an O_h complex and to the Jahn–Teller E_g mode, is usually written as

$$H_{el-ph} = V_E \begin{pmatrix} \frac{1}{2} & 0 & 0 \\ 0 & \frac{1}{2} & 0 \\ 0 & 0 & -1 \end{pmatrix} Q_\theta + V_E \begin{pmatrix} -\sqrt{3}/2 & 0 & 0 \\ 0 & +\sqrt{3}/2 & 0 \\ 0 & 0 & 0 \end{pmatrix} Q_\varepsilon \qquad (4)$$

where the normal coordinates Q_θ and Q_ε of the complex transform respectively as $3z^2 - r^2$ and $x^2 - y^2$. In a pure tetragonal distortion $Q_\varepsilon = 0$, and the separation ΔE_{sd} between the singlet and the doublet electronic states is $\Delta E_{sd} = \frac{3}{2} V_E Q_\theta$, where $Q_\theta = (2\sqrt{3}/3)(R_{ax} - R_{eq})$ (denoting by R_{ax} and R_{eq} the axial and equatorial metal–ligand distances, respectively). From the measurements under stress on the $^4T_{1g}(G)$ state Solomon and McClure [25] reported a value of $V_E = 66\ cm^{-1}\ pm^{-1}$ for $RbMnF_3$.

Therefore, assuming the same V_E value for $RbCdF_3:Mn^{2+}$, and taking $R_{ax} - R_{eq} = 0.2$ pm at 20 K, a value of $\Delta E_{sd} = 23\ cm^{-1}$ is found, which is smaller than the spin–orbit interaction $\zeta = 300\ cm^{-1}$ of Mn^{2+}, and two orders of magnitude smaller than the experimental bandwidth. This small value of the tetragonal splitting explains the similarity between the excitation and emission spectra found in the cubic and tetragonal phases of $RbCdF_3:Mn^{2+}$ and justifies the absence of splitting in the low-temperature spectra. Furthermore the present reasoning suggests that even if $|R_{ax} - R_{eq}| \simeq 2$ pm no splitting should be observable in the $^4T_1(G)$ band, as is in fact verified for MnF_2 [26].

Below $T_c = 124$ K, the tetragonal geometry would give rise to a splitting of the $^4T_{1g}(G)$ state. As the separation between such sublevels at $T = 100$ K should be clearly smaller than kT, it leads to the conclusion that changes experienced by $M_1(T)$ in the vicinity of T_c can hardly be ascribed to population effects in the sublevels arising from the $^4T_{1g}(G)$ manifold. By contrast, they can reasonably be assigned to the changes experienced by the centre of gravity of such sublevels.

3.5. Microscopic insight into $M_1(T)$ for $T > T_c$

If we consider a MnF_6^{4-} complex embedded in a host crystal such as $RbCdF_3$, the first moment M_1 (which essentially corresponds to the maximum of the emission band) strongly depends on the metal–ligand distance R [7]. Nevertheless the temperature dependence of M_1 cannot be ascribed only to the variations of R as consequence of thermal expansion effects [27,28]. This important idea can be well understood using thermodynamic arguments for a *collection* of isolated MnF_6^{4-} complexes embedded in a given lattice. In fact, assuming that M_1 is a function of R and T, it can be written

$$(\partial M_1/\partial T)_P = (M_1')_i + (M_1')_e \qquad (5)$$

with

$$(M_1')_i = (\partial M_1/\partial R)_T (\partial R/\partial T)_P = R\alpha_L (\partial M_1/\partial R)_T$$

and

$$(M_1')_e = (\partial M_1/\partial T)_R$$

where α_L is the *local* thermal expansion coefficient. The first term, called the implicit contribution, reflects the local thermal expansion effects, while the second one, called the explicit contribution, accounts for the changes in M_1 due to temperature variations *but* keeping the metal–ligand distance constant.

In the case of optical transitions, an explicit contribution to the transition energy appears because the vibrational frequencies associated with excited states, ω_{ex}^j, and the electronic ground state, ω_g^j, are usually different [29]. This phenomenon, which is specially important for the vibrational modes of the complex, gives rise to the following contribution to $M_1(T)$:

$$(M_1)_{ee} = \sum_j \left\{ \frac{(\omega_e^j)^2 - (\omega_g^j)^2}{(\omega_g^j)^2} \right\} \hbar\omega_g^j (\bar{n}_j + \tfrac{1}{2}) \tag{6}$$

where $\bar{n}_j$ is the Bose–Einstein occupancy factor associated with mode j. The actual importance of this contribution is hard to evaluate *a priori*.

(6) resembles the microscopic description of the thermal expansion undergone by a molecule or a solid. In the latter case, however, the factor in curly brackets has to be replaced by the Grünneisen coefficient, γ_j, associated with mode j [30]. Moreover, if we want to calculate the contribution $(M_1')_{ee}$ to $(M_1')_e$, one should consider factors such as $(\partial\omega_g^j/\partial T)_R$, where thermal expansion effects are then excluded. As an *a priori* evaluation of (6) is certainly hard to accomplish, a rough approximation is sometimes used. Assuming that the expression in curly brackets in (6) is j independent [31], $(M_1)_{ee}$ can be related to the lattice internal energy $U_L(T)$ as follows:

$$(M_1)_{ee} = \beta U_L(T) \qquad \text{with } \beta = (\omega_e^2 - \omega_g^2)/\omega_g^2. \tag{7}$$

Therefore, within this approximation, and assuming that β is temperature independent,

$$(M_1')_{ee} = \beta C_V(T). \tag{8}$$

In the present case of electric dipole phonon-assisted transitions, there is a supplementary contribution to $(M_1')_e$. In fact, M_1 experiences a variation with T reflecting the temperature changes undergone by both phonon creation and annihilation processes [32]. Such a variation can be written for an effective odd mode as follows:

$$(M_1)_{eu} = -\hbar\omega_u \tanh(\hbar\omega_u/2kT). \tag{9}$$

Therefore, within this theoretical framework, $(M_1')_e$ is given by

$$(M_1')_e = (M_1')_{ee} + (M_1')_{eu} \tag{10}$$

where $(M_1')_{eu} = (\partial(M_1)_{eu}/\partial T)_R$.

Let us now focus on the experimental value, $(\partial M_1/\partial T)_{P_0} = 1.88\ \text{cm}^{-1}\ \text{K}^{-1}$, found for $RbCdF_3:Mn^{2+}$ when $T > T_c$. The value of the implicit contribution can be calculated using $(\partial M_1/\partial R) = 164\ \text{cm}^{-1}\ \text{pm}^{-1}$ derived from the experimental variation of the emission peak in Mn^{2+}-doped fluoroperovskites [33]. In these systems the Mn^{2+}–F^- distance has been derived using EPR [8] and optical data [6, 7], and in the case of $KZnF_3$ and $RbCdF_3$ lattices also by EXAFS [34].

As regards the local coefficient, α_L, though not known, it is likely not far from the experimental value $\alpha = 1.2 \times 10^{-5}\ \text{K}^{-1}$ derived for $RbCdF_3$ from the crystallographic data

reported by Rousseau *et al* just above T_c [12]. In fact, the thermal expansion coefficient for diamagnetic fluoroperovskites in the cubic phase at room temperature is 1.4×10^{-5} K^{-1} for $CsCdF_3$ [12], 1.7×10^{-5} K^{-1} for $TlCdF_3$ [12] and 1.8×10^{-5} K^{-1} for $RbMnF_3$ and $KMnF_3$ [35,36]. Therefore taking $\alpha_L = 1.2 \times 10^{-5}$ K^{-1}, we calculate $(M_1')_i = 0.42$ cm^{-1} K^{-1}, which is certainly smaller than the experimental value $(\partial M_1/\partial T)_{P_0} = 1.88$ cm^{-1} K^{-1}. Thus it becomes clear that this variation cannot be explained only through thermal expansion effects in spite of the uncertainties in the actual α_L value. Furthermore the present results support that $(\partial M_1/\partial T)_{P_0}$ for the *emission* band of MnF_6^{4-} in the cubic phase of $RbCdF_3$ is clearly dominated by the explicit $(M_1')_e$ term. A rather similar conclusion to the present one was reached in the analysis of the temperature dependence displayed by the $^6A_1(S) \rightarrow {}^4T_1(G)$ *absorption* peak in $RbMnF_3$ and $KMnF_3$ [28].

The contribution $(M_1')_{eu}$ to $(M_1')_e$ around 200 K is $+0.55$ cm^{-1} K^{-1} for $\hbar\omega_u = 260$ cm^{-1}. Therefore, taking into account (5) and (10), it appears that the contribution $(M_1')_{ee}$ to $(\partial M_1/\partial T)_P$ should be about 0.9 cm^{-1} K^{-1}, and thus it is the dominant contribution to $(\partial M_1/\partial T)_P$.

3.6. Microscopic insight into the jump undergone by $(\partial M_1/\partial T)_{P_0}$ at T_c

From the analysis given in subsection 3.5, the jump experienced by $(\partial M_1/\partial T)_{P_0}$ on going from the cubic to the tetragonal phase can be written as $\Delta_t(\partial M_1/\partial T)_{P_0} = \Delta_t(M_1)_i + \Delta_t(M_1')_{eu} + \Delta_t(M_1')_{ee}$, where Δ_t is defined in (1). The first contribution is related to the jump, $\Delta_t\alpha_L$, undergone by the linear thermal expansion coefficient through the equation

$$\Delta_t(M_1')_i = R(\partial M_1/\partial R)\Delta_t\alpha_L. \tag{11}$$

Therefore the relative variation $[\Delta_t(M_1')_i]/(M_1')_i$ should be equal to $\Delta_t\alpha_L/\alpha_L$. From the data reported by Rousseau *et al* [12] it is found that $\alpha_L = 1.8 \times 10^{-5}$ K^{-1} below T_c in the 120–100 K range, thus implying $\Delta_t\alpha_L/\alpha_L \sim 0.4$. This significant variation experienced by α_L leads to a contribution $\Delta_t(M_1')_i = 0.2$ cm^{-1} K^{-1}. Therefore this contribution *alone* not only explains the positive sign of the experimental jump but also provides a figure that is certainly close to $\Delta_t(\partial M_1/\partial T)_{P_0} = 0.23$ cm^{-1} K^{-1} reported in subsection 3.3. This situation is amazing as $(M_1')_i$ is not the dominant contribution to $(\partial M_1/\partial T)_P$ in the cubic phase as discussed in subsection 3.5.

Let us, however, explore what jumps are expected arising from the two explicit contributions, $(M_1')_{eu}$ and $(M_1')_{ee}$. Having in mind that an optical frequency such as ω_u does not experience a jump at a second-order phase transition, $(M_1')_{eu}$ should be connected to $\Delta_t(\partial\hbar\omega_u/\partial T)_R$. In the case of fluoroperovskites $\Delta_t(\partial\hbar\omega_u/\partial T)_P \sim 10^{-2}$ cm^{-1} K^{-1} for odd optical modes lying below 300 cm^{-1} [24]. Therefore it is rather reasonable to accept that $\Delta_t(M_1')_{eu}$ would certainly be much smaller than the experimental value $(\partial M_1/\partial T)_{P_0} = 0.22$ cm^{-1} K^{-1}. An estimation of $\Delta_t(M_1')_{ee}$ can be reached through the rough approximation depicted in (8), which gives rise to

$$\Delta_t(M_1')_{ee}/(M_1')_{ee} = \Delta_t C_V/C_V. \tag{12}$$

Assuming $\Delta_t C_V/C_V = \Delta_t C_P/C_P$, we obtain from the experimental results reported for $TlCdF_3$ and $RbCaF_3$ [13] values of $\Delta_t C_P/C_P < 0.05$ for $t \sim 20$ K. The latter value, which is an order of magnitude smaller than $\Delta_t\alpha_L/\alpha_L$, reflects very similar values of C_P at $T_c + 20$ K and $T_c - 20$ K, in spite of the detectable lambda peak displayed by C_P in the PT region. Having in mind (12), we thus estimate $\Delta_t(M_1')_{ee} = 0.04$ cm^{-1} K^{-1}. Therefore even considering the roughness of this estimation we can understand why $\Delta_t(M_1')_i$ can be

the dominant contribution to the experimental jump $\Delta_t(M_1')$ although M_1' in the cubic phase is strongly dominated by $(M_1')_{ee}$.

It is worth noting that even taking into account the relative jump $\Delta_0 C_P/C_P$ experienced by C_P at the PT temperature, it amounts only to 0.2, which is still certainly smaller than the corresponding value $\Delta_0\alpha_L/\alpha_L = 0.75$. This significant difference between $\Delta_0\alpha_L/\alpha_L$ and $\Delta_0 C_P/C_P$ probably reflects the important changes undergone by the Grüneisen parameters (as pointed out in [11]), which influence $\Delta_0\alpha_L$ but not $\Delta_0 C_P$. The bigger relative jump experienced by α_L when compared to that of C_P at the PT of $RbCdF_3$ is consistent with Ehrenfest equations and measurements on elastic constants.

In fact, using Ehrenfest's equations for second-order phase transitions, together with the well known approximation $\alpha_L = \frac{1}{3}\chi\gamma C_V$ for the thermal expansion coefficient in the cubic phase, the following expression is obtained:

$$(\Delta_0 C_P/C_P)(\Delta_0\chi/\chi) = 3T_c\gamma\Delta_0\alpha_L(\Delta_0\alpha_L/\alpha_L). \tag{13}$$

This expression thus relates the relative jump experienced by the thermal expansion coefficient to the corresponding ones undergone by the compressibility, χ, and the specific heat, C_P. Introducing into (13) the values $\alpha_L = 1.3 \times 10^{-5}\ K^{-1}$, $\Delta_0\alpha_L = 10^{-5}\ K^{-1}$, $T_c = 124$ K, and taking $\gamma = 2.5$, we obtain

$$(\Delta_0 C_P/C_P)(\Delta_0\chi/\chi) = 0.007 \tag{14}$$

a figure which suggests that this relative jump experienced by C_P and χ at the phase transition would be certainly smaller than $\Delta_0\alpha_L/\alpha_L \sim 0.7$. This conclusion is supported by the specific heat measurements (giving $\Delta_0 C_P/C_P \sim 0.25$) and by data on the temperature dependence of elastic constants. In the case of $RbCdF_3$ only $\Delta_0 C_{11}/C_{11} = -0.05$ has been measured. From that value $\Delta_0\chi/\chi = 0.05$ can be estimated, which is close to what is predicted through (13).

4. Conclusions

A careful analysis of the temperature dependences of the emission spectrum and lifetime of Mn^{2+} impurities embedded in $RbCdF_3$ has shown that the Mn^{2+} luminescence feels the PT of the host lattice.

As a main conclusion, this work has pointed out that the jump $\Delta_t(\partial M_1/\partial T)_{P_0}$ is determined mainly by the corresponding jump associated with $(M_1')_i$ though the extrinsic contribution, $(M_1')_e$, to $(\partial M_1/\partial T)_{P_0}$ is the dominant one in the cubic phase. This fact would be of consequence of the significant relative increase, $\Delta_t\alpha_L/\alpha_L$, undergone by the thermal expansion coefficient. Additional contributions to this jump associated with the tetragonal symmetry of the complex below T_c have been ruled out given that accurate ENDOR results reported by Studzinski and Spaeth [4] indicate that at $T = 30$ K the local geometry of the MnF_6^{4-} complex is essentially cubic.

In conclusion, this work has shown not only that the luminescence of the Mn^{2+} impurity is sensitive to the second-order PT undergone by $RbCdF_3$, but also that it is possible to understand the mechanisms giving rise to the jump of $(\partial M_1/\partial T)_{P_0}$ observed at the PT.

Acknowledgments

Thanks are due to J P Chaminade for useful work in crystal growing. Fruitful discussions with M Couzi and J M Pérez-Mato are acknowledged. This work has been supported by the CYCIT under project No PB 92-0505.

References

[1] Sturge M D 1973 *Phys. Rev.* B **8** 6
[2] Rousseau J J, Leblé A and Fayet J C 1978 *J. Physique* **39** 1215
[3] Knierim W, Honold A, Brauch U and Dürr U 1986 *J. Opt. Soc. Am.* B **3** 119
[4] Studzinski P and Spaeth J M 1986 *J. Phys. C: Solid State Phys.* **19** 6441
[5] Villacampa B, Casas González J, Alcalá R and Alonso P J 1991 *J. Phys.: Condens. Matter* **3** 8281
[6] Rodríguez F and Moreno M 1986 *J. Chem. Phys.* **84** 692
[7] Marco de Lucas M C, Rodríguez F and Moreno M 1993 *J. Phys.: Condens. Matter* **5** 1437
[8] Barriuso M T and Moreno M 1984 *Phys. Rev.* B **29** 3623
[9] Shirane G, Minkiewicz V J and Linz A 1970 *Solid State Commun.* **8** 1941
[10] Lehner N, Rauh H, Strobel K, Geick R, Heger G, Bouillot J, Renker B, Rousseau M and Stirling W G 1982 *J. Phys. C: Solid State Phys.* **15** 6545
[11] Ridou C, Rousseau M, Bouillot J and Vettier C 1984 *J. Phys. C: Solid State Phys.* **17** 1001
[12] Rousseau M, Gesland J Y, Julliard J, Nouet J, Zarembowitch J and Zarenbowitch A 1975 *Phys. Rev.* B **12** 1579
[13] Chabin M, Gilleta F and Ridou C 1978 *Phys. Status Solidi* a **48** 67
[14] Ridou C 1979 *Thèse d'Etat* Université du Paris VI
[15] Marco de Lucas M C, Rodríguez F, Dance J M, Moreno M and Tressuad A 1991 *J. Lumin.* **48 & 49** 553
[16] Breñosa A G, Moreno M, Rodríguez F and Couzi M 1991 *Phys. Rev.* B **44** 9859
[17] Losada M A, Alcalá R, Alonso P J, Cases R and Orera V M 1988 *Radiat. Eff. Express* **2** 39
[18] Marco de Lucas M C and Rodríguez F 1990 *Rev. Sci. Instrum.* **61** 23
[19] Lee K H and Sibley W A 1975 *Phys. Rev.* B **12** 3392
[20] Marco de Lucas M C, Rodríguez F and Moreno M 1994 *Phys. Status Solidi* b at press
[21] Rodríguez F, Riesen H and Güdel H U 1991 *J. Lumin.* **50** 101
[22] Kamitakahara W A and Rotter C A 1975 *Solid State Commun.* **17** 1350
[23] Rousseau M, Gesland J Y, Hennion B, Heger G and Renker B 1981 *Solid State Commun.* **38** 45
[24] Ridou C, Rousseau M and Gervais F 1986 *J. Phys. C: Solid State Phys.* **19** 5757
[25] Solomon E I and McClure D S 1974 *Phys. Rev.* B **9** 4690
[26] Goldberg V, Moncorgé R, Pacheco D and Di Bartolo B 1978 *Luminescence of Inorganic Solids* ed B Di Bartolo (New York: Plenum) p 603
[27] Walsh W M, Jeener J and Bloembergen N 1965 *Phys. Rev.* **139** A1338
[28] Rodríguez F, Moreno M, Dance J M and Tressaud A 1989 *Solid State Commun.* **69** 67
[29] Ballhausen C J 1979 *Molecular Electronic Structures of Transition Metal Complexes* (New York: McGraw-Hill)
[30] Ashcroft N W and Mermin N D 1976 *Solid State Physics* (New York: Holt, Rinehart and Winston)
[31] McCumber D E 1964 *Phys. Rev.* **134** A299
[32] Di Bartolo B 1968 *Optical Interactions in Solids* (New York: Wiley)
[33] Marco de Lucas M C, Rodríguez F and Moreno M 1993 *Proc. XII Conf. on Defects in Insulating Materials (Nordkirchen, 1992)* vol 1, ed O Kanert and J M Spaeth (London: World Scientific) p 248
[34] Leblé A 1982 *Thèse d'Etat* Univerité du Maine
[35] De Jongh L J and Breed D J 1974 *Solid State Commun.* **15** 1061
[36] Dorman E, Copley J R D and Jaccarino V 1977 *J. Phys. C: Solid State Phys.* **10** 2767